A Mode Steering Antenna for Vehicular to LEO Satellite Communication

Haiyang Wang, Yue Li, *Senior Member, IEEE*, Dawei Zhou, and Zhijun Zhang, *Fellow, IEEE*

***Abstract*—In this correspondence, a mode steering antenna for low-earth orbit (LEO) satellite communication (SatCom) is proposed. Unlike traditional dual-antenna beam steering, two ports share a metal sheet. By adjusting the phase difference (PD) between the two ports, the radiation pattern is steered, thereby enabling stable communication links between the LEO satellite and the vehicle. Exciting the two ports with common-mode (CM) and differential-mode (DM) excitations induces orthogonal current distributions on the metal sheet, achieving complementary radiation patterns. Adjusting the PD between two ports in 45° intervals, the spatial coverage rate of the antenna is further enhanced. Simulated results indicate that 80% of the space area has a gain exceeding −2 dBic. A prototype was fabricated and measured to validate the concept. The measured impendence bandwidth with $S_{11} < -10$ dB and $S_{21} < -15$ dB cover the band 1.45–1.55 GHz. The proposed antenna exhibits significant potential in the LEO SatCom systems for vehicles with glass rooftops.**

***Index Terms*—Common-mode (CM), differential-mode (DM), LEO SatCom, mode steering, phase difference (PD), spatial coverage rate.**

I. Introduction

Internet of Vehicles (IoV) makes the vehicle a key component in the communication network. Communication between vehicles and base stations is the most common form of communication in vehicular networks [1], [2], [3]. But ground-based mobile systems cover only 6% of the Earth's area, which corresponds to 20% of the land area [4]. Enabling communication between vehicles and satellites in areas where base station coverage is unavailable is a hot research topic.

Satellites are classified into geostationary (GEO), medium Earth orbit, and low Earth orbit (LEO) satellites based on their orbital altitude. Due to the high orbital altitude of GEO, communication delay is significantly higher, and the limited number of GEO satellites results in constrained communication speed [5]. Due to the long communication distance, high-gain antennas are required to achieve GEO satellite communication (SatCom). Additionally, since satellite emitted electromagnetic waves are circularly polarized (CP), CP antennas are often designed to avoid polarization mismatch [6], [7], [8], [9], [10], [11], [12]. The folded dipole mode and loop mode of the loop antenna [8] were excited to achieve CP. In [11], a crossed dipole structure is used to achieve CP, and parasitic elements are introduced to enhance the bandwidth.

Received 23 January 2025; revised 28 April 2025 and 5 June 2025; accepted 29 June 2025. Date of publication 4 July 2025; date of current version 18 December 2025. This work was supported by the National Natural Science Foundation of China under Contract 62271279. The review of this article was coordinated by Prof. Wensong Wang. *(Corresponding author: Zhijun Zhang.)*

Haiyang Wang, Yue Li, and Zhijun Zhang are with the Department of Electronic Engineering, Tsinghua University, Beijing 100084, China, and also with the Beijing National Research Center for Information Science and Technology, Tsinghua University, Beijing 100084, China (e-mail: zjzh@tsinghua.edu.cn).

Dawei Zhou is with Honor Device Company Ltd., Beijing 100095, China (e-mail: zhoudawei@hihonor.com).

Digital Object Identifier 10.1109/TVT.2025.3585972

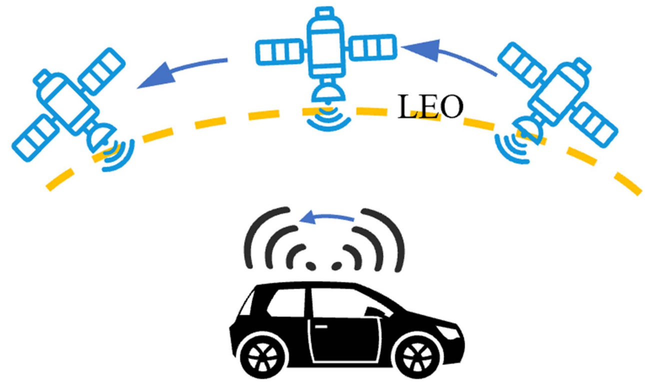

Fig. 1. Schematic of LEO SatCom between ground communication devices such as vehicles.

In recent years, LEO satellites have developed rapidly. Compared to GEO satellites, LEO satellites are more numerous, offering significantly higher communication speeds, and lower latency. However, the position of LEO satellites relative to the Earth is not fixed and changes over time. Ground antennas must either achieve full-space coverage or implement beam scanning to provide stable SatCom as shown in Fig. 1. Currently, SatCom can be achieved in both the millimeter-wave (mmW) and sub-6G frequency bands. The mmW band provides high-speed communication, while the sub-6G band supports lower-speed communication. Extensive high-gain mmW arrays for SatCom has been published [13], [14], [15], [16], [17]. Reflectarray [13] and transmitarray [14] can achieve high gain with fixed beams. In [15], [16], [17], these phased arrays can achieve beam scanning, with an elevation scanning angle of 40°.

For low-speed communication scenarios in the sub-6G band, ensuring a stable satellite connection is more important than high gain and CP. Although omnidirectional antennas [18], [19] can cover a plane, they have fixed nulls, making them unsuitable for LEO SatCom. The quadrifilar helical antenna in [20] can achieve CP over a half-sphere, but it typically has a relatively high profile. Isotropic antennas [21], [22], [23], [24] can cover different angles of LEO satellites, However, the gain of isotropic antennas is too low. Multi-port shared-radiator antennas can achieve beam scanning by adjusting the port phase differences (PDs) [25], [26], which enhances the gain of the synthesized radiation pattern. However, these antennas are 3D structures, making them unsuitable for deployment on mobile devices. Small volume and low-profile antennas [27], [28] are convenient for integration into vehicles. Therefore, it is necessary to design a planar shared-radiator antenna that provides wide spatial coverage to support LEO SatCom.

In this correspondence, the metal sheet serves as the shared-radiator structure for two ports. CM and DM excitations induce two orthogonal modes of current on the metal sheet, achieving complementary radiation patterns. Unlike traditional CP antennas used for SatCom, we are not concerned with whether the antenna forms CP at a specific angle; instead, we focus on the spatial coverage rate of gain. To further enhance the antenna spatial coverage rate, the PD between two ports is adjusted in 45° intervals. The results show that in 80% of the spatial region, the gain exceeds –2 dBic. Therefore, the proposed antenna holds strong potential for applications in LEO SatCom such as vehicles with glass rooftops.

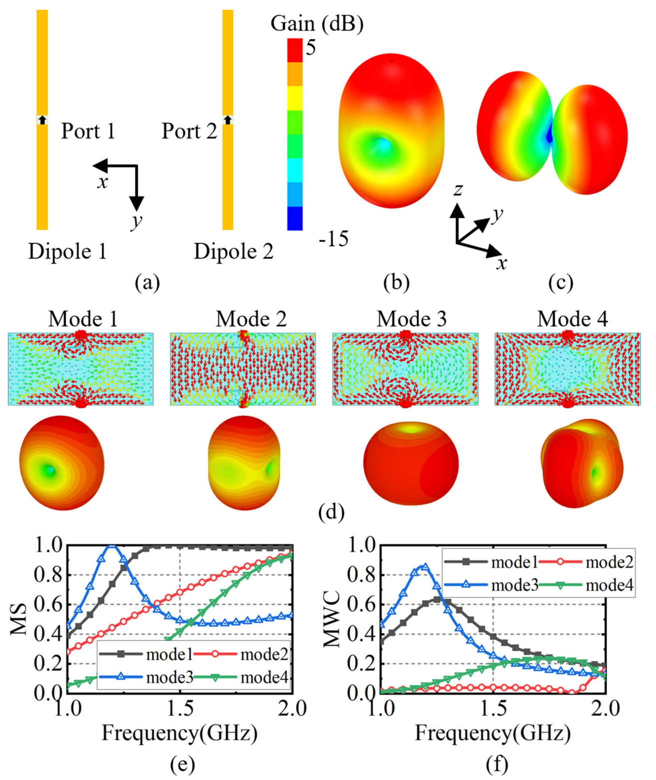

Fig. 2. (a) Schematic of conventional beam steering of two dipole antennas, (b)radiation pattern of two ports in phase; (c) Radiation pattern of two ports out of phase. (d) Modal currents on the metal sheet and radiation patterns, (e)modal significance, (f) modal weighting coefficients.

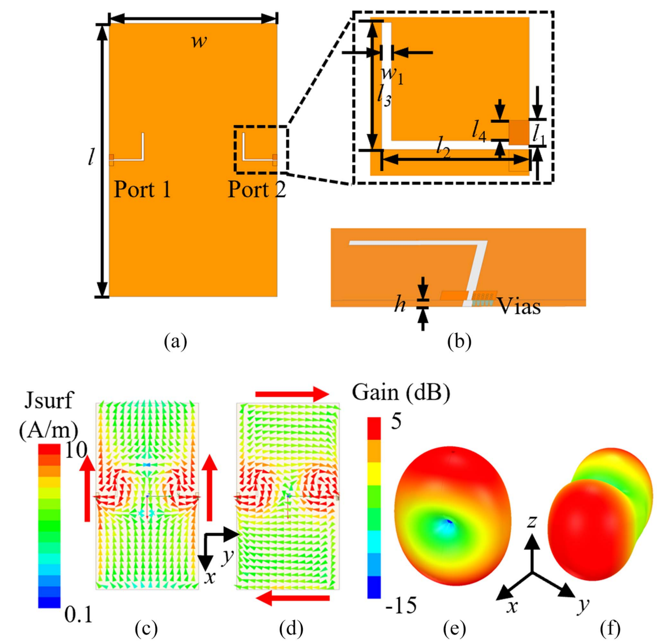

Fig. 3. Proposed antenna: Two ports are located along the long edge of the metal sheet. (a) Top view, (b) side view. $l_1 = 2.8$ mm, $l_2 = 14.5$ mm, $l_3 = 13.5$ mm, $l_4 = 2.3$ mm, $w_1 = 1$ mm, $h = 0.5$mm. (c)-(f): Current distributions and radiation patterns at 1.5 GHz. (c)(e) CM, (d)(f) DM.

II. Antenna Design Principle for LEO Satellite

In this paper, we aim to design an antenna specifically for LEO SatCom. Using multiple antennas would introduce impractical complexity. Therefore, we have designed two ports sharing the metal sheet to achieve broad coverage with spatial beam steering. To simplify the design, the amplitudes of the two ports are kept equal, and only the PD is adjusted.

A. Conventional Beam Steering Design

To highlight the innovation of this paper, conventional beam steering antenna simulated results are presented here. Fig. 2(a) depicts a schematic diagram of two dipole antennas. Adjusting the PD between ports 1 and 2 enables the steering of the radiation beam in Fig. 2(b) and (c). For simplicity, we only present the radiation patterns when the PD is 0° and 180°. While the binary dipole array can achieve beam steering by adjusting the PD, the radiation pattern of dipole element is fixed and radiation nulls along *y*-axis cannot be eliminated. The inherent nulls area cannot be used for LEO SatCom.

B. Mode Steering Strategy and CMA Analysis

Conventional array beam steering changes the array factor by adjusting the PD. However, the individual element radiation pattern does not change. We perform characteristic mode analysis (CMA) on the metal sheet in Fig. 2(d), aiming to find modes that can complement each other's radiation patterns to achieve high spatial coverage. CMA provides valuable insights into how different characteristic modes contribute to the radiation performance and enables a better understanding of the underlying beam steering mechanism. As shown in Fig. 2(d), Modes 1, 3 and 4 of the four CMA modes on the sheet achieve complementary radiation patterns. Fig. 2(e) and (f) present the modal coefficients and modal weighting coefficients under long-edge port excitation of the metal plate. Analysis of the characteristic current distributions indicates that varying the PD between the feeding ports excites different characteristic modes, which in turn results in different radiation patterns and enables beam steering. These modes steering can result in high spatial coverage.

There are various ways to excite the metal sheet modes. To validate the effectiveness of the proposed method, this paper adopts the most direct method by using a slot along the long edge of the metal sheet. Compared to traditional two-dipole antenna configurations, the mode steering method achieves improved beam coverage by overcoming the fixed radiation nulls typically observed in conventional array beam steering.

III. Antenna Design

Fig. 3(a) and (b) depicts the structure of the metal sheet with two L-shaped slots. The substrate is FR-4 ($\varepsilon r = 4.8$ and $\tan\delta = 0.02$), with a thickness of 0.5 mm. The size of bottom metal sheet is 140 mm × 70 mm. As shown in Fig. 3(b), there are two metal pieces above the slot on the top layer of the substrate. The cable is connected to the two metal pieces to excite the metal sheet current. The inset presents specific dimensions of the L-shaped slot. To reduce the length of slot on the metal sheet in the y-direction, an L-shaped slot is adopted in this correspondence. The L-shaped slot and the metal piece (without vias) serve as matching components, acting as a shunt inductance and a series capacitance, respectively.

Fig. 3(c) and (d) shows the current distribution diagrams of CM and DM excitations. Two orthogonal modes of sheet currents are being excited successfully. Fig. 3(c) shows the surface current distribution under common-mode excitation. Mode 1 is predominantly excited resulting in radiation currents primarily along the *x*-direction. In contrast, when

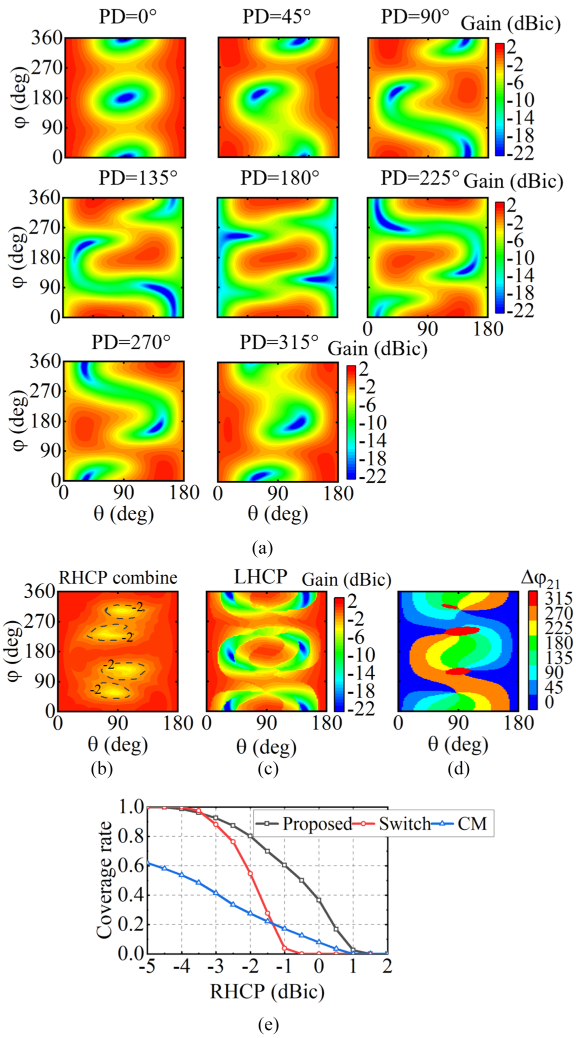

Fig. 4. Simulation radiation patterns and CDF of spatial coverage. (a) RHCP radiation patterns with the different PD of two ports. The PD values are 0°, 45°, 90°, 135°, 180°, 225°, 270° and 315°. (b) Combined RHCP gain; (c) LHCP gain (cross-polarization of Fig. 4(b); (d) The corresponding PD distribution of Fig. 4(b). (e) CDFs under three excitation methods. CM: only CM excitation; Switch: port1 and port2 switch to work.

the PD is 180°, Modes 3 and 4 are mainly excited, producing radiation currents along the y-direction in Fig. 3(d). Fig. 3(e) and (f) presents the radiation patterns of CM and DM excitations. It is evident that the main lobes and radiation nulls of the radiation patterns in the two cases are nearly complementary, which provides a solid foundation for achieving combined wide spatial coverage. However, using only these two excitations results in relatively low spatial coverage gain. Theoretically, continuous PD adjustment can achieve the best space coverage. In this paper, a minimum discrete phase of 45° is employed to further improve the coverage rate because continuous phase adjustment is not easy to achieve in practice.

A. Mode Steering and RHCP Coverage

We assume that the satellite transmits RHCP waves, so the antenna total gain does not directly reflect the actual SatCom gain. Therefore, the RHCP gain of the antenna represents the effective communication gain with the satellite. In this work, eight radiation patterns are obtained under eight different PD excitations. Fig. 4 illustrates the RHCP gain

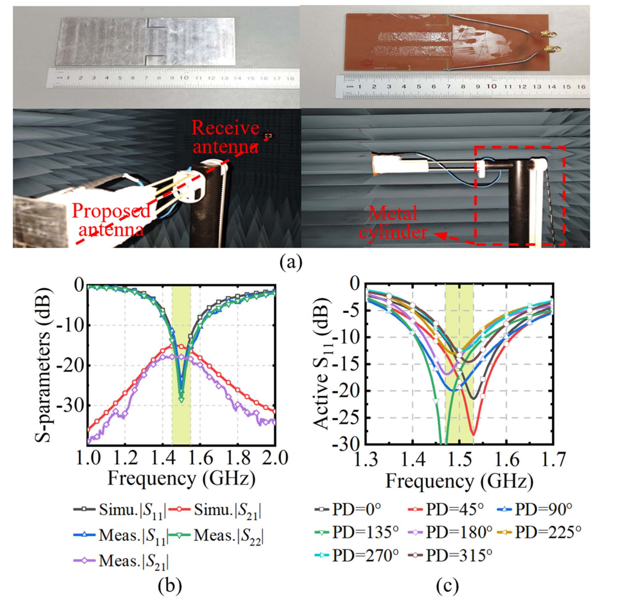

Fig. 5. Fabricated prototype and antenna testing. (a) Fabricated prototype of the proposed antenna and antenna testing environment, (b) measured S-parameters, (c) active S_{11}.

patterns corresponding to these eight PDs. It can be seen that the direction of the main beam varies with the different PDs. The combined radiation pattern shown in Fig. 5(a) is derived using the formulation (1).

$$[\text{RHCP\_combine}(\theta,\varphi), \text{index}] = \max\,[1,\ldots\ldots,8] \tag{1}$$

The indices 1 to 8 in (1) correspond to the eight PD cases illustrated in Fig. 4(a). The "RHCP_combine(θ,φ)" refers to the synthesized result shown in Fig. 4(b). The "index" records the required PD corresponding to the maximum gain at each spatial angle shown in Fig. 4(d).

Fig. 4(b) represents the combined RHCP gain pattern obtained by selecting the maximum value at each spatial direction from the eight radiation patterns presented in Fig. 4(a). The region inside the dashed circle indicates the gain of less than −2 dBic. It can be observed that there are no radiation nulls in the entire space, and the RHCP gain in most regions can achieve -2 dBic or higher.

Fig. 4(c) provides the LHCP gain which is the cross-polarization of Fig. 4(b). As widely known, when the LHCP gain is equal to the RHCP gain, the radiated electromagnetic waves are linear polarization. When the RHCP gain is greater than the LHCP gain, the radiated electromagnetic waves are primarily RHCP. By comparing Fig. 4(b) and (c), it can be observed that only a small portion of the spatial directions exhibit circular polarization, while the majority of the radiation regions are either elliptically or linearly polarized. The antenna predominantly exhibits linear polarization (LP) because, at PDs of 0° and 180°, the excited polarization states are primarily x-polarization and y- polarization, respectively. CP can be observed in certain spatial directions when other phase difference excitations, such as 90°, are applied. Under such conditions, both x-polarized and y-polarized currents are simultaneously excited. In these directions, the orthogonal current components exhibit a phase difference close to 90° and comparable amplitudes, resulting in favorable CP radiation. However, it should be noted that this CP is not a result of intentional design, but rather an incidental outcome of the antenna structure.

It should be noted that we are not concerned with whether the antenna radiates CP or LP waves. We are only concerned with whether the RHCP gain in space is sufficient for LEO SatCom. In LEO SatCom, RHCP gain of -2 dBic or higher is sufficient to maintain communication. Fig. 4(d) shows the phase distribution corresponding to the combined gain pattern in Fig. 4(b). We can observe that different PDs are required for different angles in space to enhance gain. In practical applications, this phase distribution can be used to dynamically track and cover satellites in real time. It should be noted that while wide spatial coverage is achieved via adjustable PD between the two feeding ports, the antenna communicates with LEO satellites in a specific beam direction at any given moment, determined by the configured PD state.

To illustrate the spatial coverage capability of the proposed method, Fig. 4(e) presents the cumulative distribution functions (CDF) of the Fig. 4(b). The region where the RHCP gain is greater than -2 dBic covers 80% of the entire space, and the region where it is greater than -4 dBic covers 99%. To further illustrate the effectiveness of PD control in enhancing spatial coverage, Fig. 4(e) also presents the cumulative distribution functions (CDFs) for two baseline cases: (1) CM: only CM excitation and (2) Switch: ports switching excitation, both using the same antenna structure. Compared with these two methods, the proposed method demonstrates a significant advantage in spatial coverage. The proposed method achieves 60% coverage rate at -1 dBic while the switch excitation achieves only 4%. Compared with only CM excitation, the coverage rate of the proposed antenna significantly increases under same gain.

B. Communication Outage Probability

The purpose of achieving wide spatial coverage is to ensure stable communication with LEO satellites. The communication outage probability is used as a metric to quantify communication stability. In LEO SatCom, it is common to observe more than one satellite. The communication outage probability between the proposed antenna and multiple satellites can be calculated using the following formula.

$$P_{out} = (1 - p)^N \tag{2}$$

P_{out} describes the communication outage probability under different numbers of LEO satellites. p represents the communication probability between the proposed antenna and a satellite, N is the number of the random LEO satellites in the space. The proposed antenna achieves a gain greater than -2 dBic in 80% of full space. Therefore, $p = 0.8$. For a single LEO satellite condition, $P_{out} = 0.2$; for two LEO satellites condition, $P_{out} = 0.04$; for three LEO satellites condition, $P_{out} = 0.008$. The low outage probabilities observed under various satellite visibility scenarios confirm that the proposed antenna ensures stable and reliable communication performance.

IV. Simulated and Measured Results

To validate the performance of the proposed mode steering mechanism, the antenna was fabricated and tested in Fig. 5(a).

A. S-Parameters

The measured S-parameters are consistent with the simulated results. The measured reflection coefficients of two ports are better than -10 dB across the 1.45 to 1.55 GHz in Fig. 5(b). The measured isolation is higher than 17 dB across the matching band. Within the frequency range of 1.47–1.53 GHz, the active $|S_{11}|$ is below -10 dB in Fig. 5(c).

B. Radiation Performance

The radiation patterns of the two ports were measured and then combined under different PDs to generate the results shown in Fig. 6(a)–(d). Fig. 6(a) presents the measured radiation patterns under different PD excitations. The results demonstrate that beam steering is achieved, and the combined radiation patterns provide wide spatial coverage. Fig. 6(b)–(d) show the measured results corresponding to Fig. 4(b)–(d), including the combined RHCP gain, cross-polarization levels, and PD distribution. Fig. 6(d) shows the PD distribution of measured combined RHCP gain. It is visually evident that in most regions, the PD aligns with the simulated result in Fig. 4(d). Comparing the measured results with the simulated, there is overall consistency, but some differences exist, such as PD = 315°. This is because a supporting metal cylinder in the anechoic chamber affects the antenna radiation patterns as shown in Fig. 5(a).

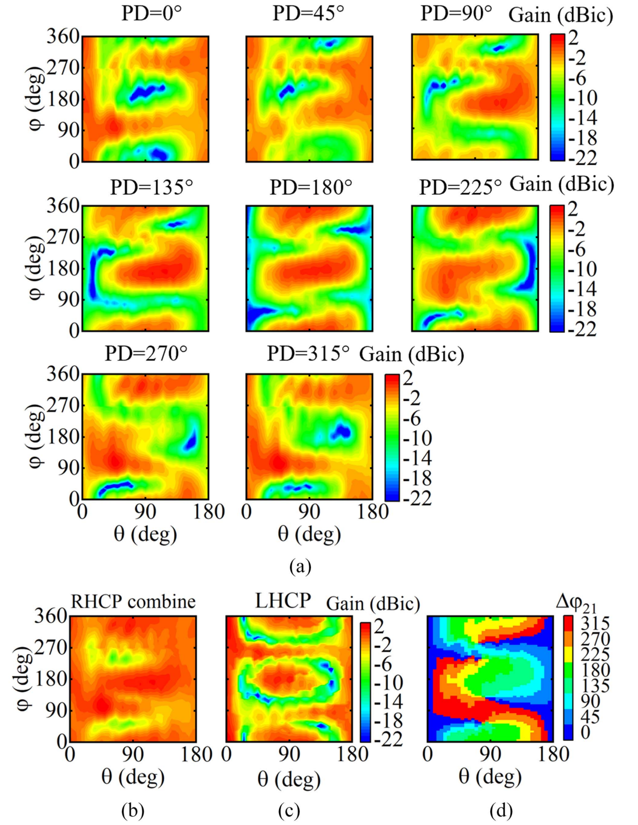

Fig. 6. (a) Measured RHCP radiation patterns with the different PD of two ports. The PD values are 0°, 45°, 90°, 135°, 180°, 225°, 270° and 315°. (b) Combined measured RHCP gain; (c) Measured LHCP gain (cross-polarization of Fig. 6(b); (d) The corresponding PD distribution of Fig. 6(b).

C. Comparison With Previous Works

Table I presents the comparison between the proposed antenna and previous antennas for SatCom. It should be noted that the coverage reported in the referenced literature is typically estimated by integrating the beamwidths in the E- and H-plane to approximate the coverage rate. The antenna in [8] features a compact structure and achieves endfire CP on a mobile phone. However, it is not suitable for vehicular applications. References [9], [11], and [12] present CP antennas based on patch, crossed dipole, and dielectric resonator structures, respectively, for satellite communication. However, such conventional CP designs typically exhibit limited spatial coverage, making them less suitable for LEO satellite communication. The coverage performance in [8], [9], [11], and [12] still requires significant improvement. A quadrifilar helical antenna is introduced in [20] which achieves full CP coverage over the upper hemisphere but has a high profile. Compared with

TABLE I
COMPARISON OF THE PROPOSED ANTENNA AND PREVIOUS ANTENNAS FOR SATELLITE COMMUNICATION

Ref.	Ant. type	Size ($\lambda_0 \times \lambda_0$)	Profile (λ_0)	Coverage[1]	Gain (dBic)
[8]	Loop	0.46×0.06	1.17	64.6%	4.8
[9]	Patch	0.75×0.75	0.10	42.7%	5.2
[11]	Cross dipole	0.70×0.70	0.40	50.0%	5.0
[12]	Dielectric-resonator	0.84×0.64	0.17	29.3%	6.6
[20]	Quadrifilar	0.32×0.32	0.6	100%	3.2
This work	sheet	0.70×0.35	0.0025	80.9%	1.3

λ_0 is the wavelength of the lowest frequency in the free space. Coverage[1]: The proportion of the upper hemisphere where the gain exceeds −2 dBic.

the antennas reported in Table I, the proposed antenna offers wide spatial coverage and features a planar structure, making it easy to integrate on vehicle glass rooftops. It is suitable for LEO SatCom applications.

V. CONCLUSION

In this article, a shared metal sheet with two ports is proposed for LEO SatCom. CM and DM excitations induce orthogonal current modes on the metal sheet, resulting in complementary radiation patterns. Therefore, the antenna has a foundation for full spatial coverage. Adjusting the PD between two ports in 45° intervals further enhances the spatial coverage gain of the proposed antenna. Ultimately, the proposed antenna achieves a spatial coverage rate of 80% under antenna gain exceeding -2 dBic and the antenna has no radiation nulls. Both the simulated and measured results indicate that the antenna can achieve excellent spatial coverage. The proposed antenna is well-suited for use in vehicular with glass rooftops and mobile devices for LEO SatCom.

REFERENCES

[1] Z. Zhang, S.-W. Wong, Y. Wen, S.-Q. Zhang, W. Li, and Y. He, “A full-metal dual-band millimeter-wave antenna array with concomitant multifold orthogonal beamforming for V2V and V2I communications,” *IEEE Trans. Veh. Technol.*, vol. 73, no. 7, pp. 10381–10389, Jul. 2024.

[2] C. Wang, W. Cao, W. Ma, Y. Tong, and Y. Zhu, “A sigle-layer dual-band shared-aperture antenna with high gain and sidelobe suppression based on high-order mode for vehicular communications,” *IEEE Trans. Veh. Technol.*, vol. 73, no. 1, pp. 473–481, Jan. 2024.

[3] W. Wang et al., “Compact quad-element vertically-polarized high-isolation wideband MIMO antenna for vehicular base station,” *IEEE Trans. Veh. Technol.*, vol. 69, no. 9, pp. 10000–10008, Sep. 2020.

[4] S. Chen, S. Sun, and S. Kang, “System integration of terrestrial mobile communication and satellite communication —The trends, challenges and key technologies in B5G and 6G,” *China Commun.*, vol. 17, no. 12, pp. 156–171, Dec. 2020.

[5] Y. Lei, Y. Xu, C. Huang, C. Yuen, and H. Zhang, “Robust secure beamforming design for GEO-based satellite communication systems,” *IEEE Trans. Veh. Technol.*, vol. 73, no. 2, pp. 2390–2400, Feb. 2024.

[6] X. Zhang, K. Wei, Y. Li, and Z. Zhang, “A polarization reconfigurable antenna for satellite communication in foldable smartphone,” *IEEE Trans. Antennas Propag.*, vol. 71, no. 12, pp. 9938–9943, Dec. 2023.

[7] J.-Y. Deng, C.-L. Lou, Z. Chen, and Y. Zhang, “Circularly polarized horn antenna with miniaturized longitudinal dimension for vehicular satellite communications,” *IEEE Trans. Veh. Technol.*, vol. 72, no. 4, pp. 5497–5501, Apr. 2023.

[8] Z. Cao, L. Chang, Y. Li, K. Wei, and Z. Zhang, “Compact mobile terminal antenna with endfire circularly polarized beam for satellite communications,” *IEEE Trans. Antennas Propag.*, vol. 71, no. 12, pp. 9980–9985, Dec. 2023.

[9] C.-F. Liang, Y.-P. Lyu, D. Chen, and C.-H. Cheng, “Wideband circularly polarized stacked patch antenna based on TM_{11} and TM_{10},” *IEEE Trans. Antennas Propag.*, vol. 70, no. 4, pp. 2459–2467, Apr. 2022.

[10] P. Wang, J. Liu, C. Zhou, B. Yin, and W. Wang, “Dual-band dual-circularly polarized fabry-pérot cavity MIMO antenna using CMM-based polarization converter and MMA for vehicular satellite communications,” *IEEE Trans. Veh. Technol.*, vol. 72, no. 7, pp. 8844–8856, Jul. 2023.

[11] Z. Chen, H. Zhu, L. H. Ye, and W. Wang, “Ultra-wideband dual-circularly polarized crossed-dipole antenna with stripline coupler and parasitic elements for vehicular sensing and communications,” *IEEE Trans. Veh. Technol.*, vol. 73, no. 6, pp. 8197–8206, Jun. 2024.

[12] H. Xu et al., “Single-fed dual-circularly polarized stacked dielectric resonator antenna for K/Ka-band UAV satellite communications,” *IEEE Trans. Veh. Technol.*, vol. 71, no. 4, pp. 4449–4453, Apr. 2022.

[13] C. Zhang et al., “A planar integrated folded reflectarray antenna with circular polarization,” *IEEE Trans. Antennas Propag.*, vol. 65, no. 1, pp. 385–390, Jan. 2017.

[14] X. Tong et al., “An integrated dual-band dual-circularly polarized shared-aperture transmit-array antenna for K-/Ka-band applications enabled by polarization twisting elements,” *IEEE Trans. Antennas Propag.*, vol. 71, no. 6, pp. 4955–4966, Jun. 2023.

[15] H. Al-Saedi et al., “An integrated circularly polarized transmitter active phased-array antenna for emerging Ka-band satellite mobile terminals,” *IEEE Trans. Antennas Propag.*, vol. 67, no. 8, pp. 5344–5352, Aug. 2019.

[16] H. Al-Saedi et al., “A low-cost Ka-band circularly polarized passive phased-array antenna for mobile satellite applications,” *IEEE Trans. Antennas Propag.*, vol. 67, no. 1, pp. 221–231, Jan. 2019.

[17] Y. Zhang, W. Hong, Z. Ding, L. Yang, C. Zhu, and Y. Hu, “Circularly polarized metasurface phased array antenna system with wide axial-ratio beamwidth for LEO mobile satellite communication,” *IEEE Trans. Antennas Propag.*, vol. 71, no. 6, pp. 4823–4833, Jun. 2023.

[18] Y. M. Pan, S. Y. Zheng, and W. Li, “Dual-band and dual-sense omnidirectional circularly polarized antenna,” *IEEE Antennas Wireless Propag. Lett.*, vol. 13, pp. 706–709, 2014.

[19] Y. Zhang, Y. Li, W. Zhang, Z. Zhang, and Z. Feng, “Omnidirectional antenna diversity system for high-speed onboard communication,” *Engineering*, vol. 11, pp. 72–79, Apr. 2022.

[20] K. Mo, X. Jiang, L. Peng, and R. Fang, “Dual-sleeves printed quadrifilar helix antenna with quad-band and ultrawide beamwidth for satellite communication mobile terminals,” *IEEE Trans. Antennas Propag.*, vol. 73, no. 4, pp. 2395–2404, Apr. 2025.

[21] P. F. Hu, Y. M. Pan, X. Y. Zhang, and B. J. Hu, “A compact quasi-isotropic dielectric resonator antenna with filtering response,” *IEEE Trans. Antennas Propag.*, vol. 67, no. 2, pp. 1294–1299, Feb. 2019.

[22] Z. Su, K. Klionovski, R. M. Bilal, and A. Shamim, “A dual band additively manufactured 3-D antenna on package with near-isotropic radiation pattern,” *IEEE Trans. Antennas Propag.*, vol. 66, no. 7, pp. 3295–3305, Jul. 2018.

[23] Y.-M. Pan, K. W. Leung, and K. Lu, “Compact quasi-isotropic dielectric resonator antenna with small ground plane,” *IEEE Trans. Antennas Propag.*, vol. 62, no. 2, pp. 577–585, Feb. 2014.

[24] Y. Zhang and Y. Li, “Wideband isotropic antenna with miniaturized ground for enhanced 3 dB coverage ratio,” *IEEE Antennas Wireless Propag. Lett.*, vol. 21, no. 6, pp. 1253–1257, Jun. 2022.

[25] K. Wang et al., “A novel phase mode antenna with triport and its application in a 1-D generalized phased array to 2-D scanning,” *IEEE Trans. Antennas Propag.*, vol. 71, no. 10, pp. 8072–8087, Oct. 2023.

[26] J. Zhang et al., “Dual-port phase antenna and its application in 1-D arrays to 2-D scanning,” *IEEE Trans. Antennas Propag.*, vol. 69, no. 11, pp. 7508–7520, Nov. 2021.

[27] Y. Zhang and Y. Li, “Wideband microstrip antenna in small volume without using fundamental mode,” *Electromagn. Sci.*, vol. 1, no. 2, pp. 1–6, Jun. 2023.

[28] N.-W. Liu, L. Zhu, W.-W. Choi, and X. Zhang, “A low-profile differentialfed patch antenna with bandwidth enhancement and sidelobe reduction under operation of TM_{10} and TM_{12} modes,” *IEEE Trans. Antennas Propag.*, vol. 66, no. 9, pp. 4854–4859, Sep. 2018.